

Dynamic pyroelectric enhancement of homogeneous ferroelectric materials

G. Akcay^a, S. Zhong^a, S.P. Alpay^{a,*}, J.V. Mantese^b

^a Department of Materials Science and Engineering and Institute of Materials Science, University of Connecticut, Storrs, CT 06269, USA

^b Delphi Research Laboratories, Shelby Township, MI 48315, USA

Received 28 September 2005; received in revised form 9 December 2005; accepted 13 January 2006 by A. Pinczuk

Available online 2 February 2006

Abstract

The time-dependent thermal response to a step-wise temperature increase of a ferroelectric plate of BaTiO₃ of finite thickness was determined using a combination of basic heat transfer relations to model the temperature variation in the ferroelectric as a function of time and a thermodynamic model based on a modified Landau formalism to calculate the polarization profile due to the temperature gradient. An enhancement over the static pyroelectric response was revealed, having a maximum value of $-0.01 \mu\text{C}/\text{cm}^2 \text{ } ^\circ\text{C}$, for detector thicknesses in the range of 1 to 100 μm .

© 2006 Elsevier Ltd. All rights reserved.

PACS: 77.70.+a; 77.90.+k

Keywords: A. Temperature graded ferroelectrics; D. Dynamic pyroelectric response

Infrared detection employing ferroelectric sensing elements as pyroelectrics was demonstrated over 40 years ago [1]. Since that time, there have been a host of studies describing ferroelectric-based pyroelectric detectors [2,3]. The most commercially successful pyroelectric technology to date has utilized barium strontium titanate (BST) materials and a hybrid fabrication process that marries bulk ceramic with IC-silicon [4].

Conventional, uncooled, ferroelectric pyrometers have historically been operated in one of two modes: the pyroelectric mode (the subject of this paper), exploiting a change in polarization with temperature; or as dielectric bolometers. For the former case, poled or electric field biased passive capacitive elements are used as the individual pixel elements of a focal plane array (FPA), with each pixel element thermally sensitive to a portion of the scene to be imaged. The material is thermally biased (and referenced via a chopper) so that the added or diminished IR energy from the imaged scene locally raises or lowers the temperature of the dielectric material pertaining to a selected pixel element. The bias temperature is adjusted to be just below (or just above in the case of field-induced polarization) the Curie temperature of the material.

During operation, an image of the scene is projected onto the FPA causing local temperature differentials, ΔT_p , from that of the reference temperature set by the chopper. The magnitude of ΔT_p , of course, depends upon such factors as the heat capacity of the pixel, what portion of the black body radiation at a selected wavelength is absorbed by the pixel element, the thermal conductance and radiation losses from the pixel to its surroundings, and the duration of exposure time as set by the chopper window. The change in surface charge of each pixel is given simply by

$$\Delta Q = A\Delta P_S, \quad (1)$$

where A is the area of the pixel element and ΔP_S is the change in spontaneous (or induced) polarization due to a temperature change, ΔT_p . Eq. (1) is often normalized to produce an intrinsic quantity, called the pyroelectric coefficient, defined by [5]:

$$p = \frac{\Delta Q}{A\Delta T_p} = \frac{\Delta P_S}{\Delta T_p}. \quad (2)$$

Quite intriguing is the well-known observation that there is a clear difference between a pyroelectric coefficient that is determined quasi-statically from hysteresis versus temperature measurements, and those that are obtained from pulsed-illumination methods whereby the charge differential is measured as an instantaneous current spike after chopped laser illumination. In this paper we examine one such root cause for that difference. We show that the incoming radiation

* Corresponding author.

E-mail address: p.alpay@ims.uconn.edu (S.P. Alpay).

flux creates an evolving temperature gradient (and hence a commensurate polarization gradient) across the thickness of the sensing element. The polarization gradient gives rise to an internal potential that may be used for thermal detection. We are thus able to define a dynamic pyroelectric coefficient enhancement, which is a function of the thermal response time of the sensing element and amplification capacitance. We simulate the conditions of a pyrometer sensing-element using a basic heat transfer approach, the Landau theory of phase transformations, and straightforward electrostatic relations.

Consider a compositionally homogeneous ferroelectric sample of thickness L at a temperature T_1 in thermal equilibrium. It is exposed to infrared (IR) radiation on one side, instantaneously increasing the surface temperature to T_2 . We assume that this surface temperature remains constant at all times while at the other end of the sample there is no convection or radiation heat transfer from the surface. Fig. 1 shows a schematic of the system that was analyzed along with initial boundary conditions. The governing relation for the heat transfer is

$$\alpha \frac{\partial^2 T}{\partial x^2} = \frac{\partial T}{\partial t} \quad (3)$$

where $T(z,t)$ is the location and time dependent temperature, α is the thermal diffusivity given by $\alpha = k/\rho C_p$, with k the thermal conductivity, ρ the density, and C_p the heat capacity. The heat capacity and thus, the thermal conductivity depend on the temperature and the polarization. For small changes in the temperature, the variation in these two parameters can be neglected. As such, we will treat α as a constant. This

assumption effectively decouples the heat transfer relation and the subsequent Landau theory of phase transformation, which, formally, should be solved simultaneously. This significantly reduces computational difficulties.

It is clear that the incoming heat flux produces a time dependent temperature gradient across the ferroelectric. Since the spontaneous polarization of a ferroelectric is a function of temperature, a non-homogeneous distribution of the temperature across a uniform ferroelectric results in a corresponding polarization variation [6]. Assuming that the easy axis of polarization of the ferroelectric is along the z -axis such that $P_1 = P_2 = 0$, $P_3 = P(z)$ (as is the case for perovskite oxide ferroelectrics such as BaTiO_3 and PbTiO_3) and the sample is homogeneous in the other two directions (x and y), the thermodynamic potential of a temperature-graded ferroelectric can be expressed via [7,8]

$$F = \int_0^L [a_1 P^2 + a_{11} P^4 + a_{111} P^6 + \frac{B}{2} \left(\frac{dP}{dz} \right)^2 - \frac{1}{2} E_D P + F_{el}^i] dz \quad (4)$$

where a_1 , a_{11} , a_{111} and B are the free energy (Landau) expansion coefficients. a_1 is given by the Curie-Weiss law: $a_1 = (T(z,t) - T_C)/(2C\epsilon_0)$, where T_C is the Curie temperature, C is the Curie constant and ϵ_0 is the dielectric permittivity of free space. We assume that the coefficients, a_{11} and a_{111} are not temperature dependent. The Ginzburg coefficient B can be approximated as $\delta^2 |a_1|$, where δ is a characteristic length along which the polarization varies. B is positive and thus the gradient term in the above relation acts as a restoring force that serves to damp out the spatial variations in P [7,8]. The inhomogeneity in the temperature of the system is reflected through the temperature dependence of the Landau coefficients a_1 and B . An internal electric field (E_D) arises from the inhomogeneous distribution of the polarization. We note that this internal field can reach substantial values if the initial polarization mismatch between the layers of a ferroelectric heterostructure is large. It was shown that this depoling field might lead to unique properties such as dielectric enhancement and compositional symmetry breaking in simple ferroelectric bilayer heterostructures [9,10]. However, we neglect this field assuming that there exists a smooth temperature gradient such that the polarization mismatch between ‘layers’ of the temperature-graded ferroelectric is small.

The last term of Eq. (4) is the elastic energy of the built-in, position dependent stress field. This energy results from the electrostrictive coupling between the polarization and the self-strain, and has two components: (i) the biaxial elastic energy due to the variation of the self-strain along L , and (ii) the energy associated with the bending of the ferroelectric due to the inhomogeneous elastic deformation. The elastic energy can be calculated from the conditions that both the average internal stress and the average momentum of the internal stress should be zero [11,12]. A complete derivation of this elastic energy incorporating both sources has been given elsewhere [8].

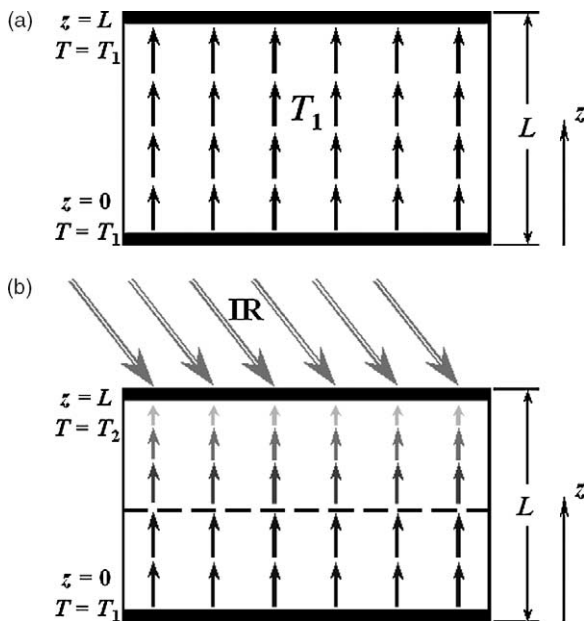


Fig. 1. (a) A schematic of the simulated system at T_1 in equilibrium, (b) One surface at T_2 immediately after the IR radiation is applied, showing the polarization gradient caused by the temperature gradient as a transient state along with the boundary conditions used in the calculations.

Accordingly

$$F_{el}^i(z) = \bar{C} \left\{ Q_{12}[P^2(z) - \langle P \rangle^2] + \left(z - \frac{L}{2} \right) \kappa \right\}^2, \quad (5)$$

where Q_{12} is the electrostrictive coefficient relating the strain in the x - y plane to polarization $P(z)$, $\bar{C} = C_{11} + C_{12} - 2C_{12}^2/C_{11}$ is an effective elastic modulus, C_{ij} are the elastic moduli at constant polarization, $\langle P \rangle$ is the average polarization

$$\langle P \rangle = \frac{1}{L} \int_0^L P(z) dz, \quad (6)$$

and κ the radius of curvature resulting from the bending moment given by:

$$\kappa = \frac{24}{L^3} \int_0^L \left(z - \frac{L}{2} \right) Q_{12}[P^2(z) - \langle P \rangle^2] dz. \quad (7)$$

Minimizing the free energy equation with respect to polarization yields the Euler-Lagrange equation [8]

$$B \frac{d^2 P}{dz^2} = \bar{a}_1 P + \bar{a}_{11} P^3 + a_{111} P^4, \quad (8)$$

with re-normalized coefficients:

$$\bar{a}_1 = a_1 + 2\bar{C}Q_{12} \left[\left(z - \frac{L}{2} \right) \kappa - Q_{12} \langle P \rangle^2 \right], \quad (9a)$$

$$\bar{a}_{11} = a_{11} + \bar{C}Q_{12}^2. \quad (9b)$$

In our analysis, we use BaTiO₃ (BT), a prototypical perovskite ferroelectric oxide. In BT, the TiO₆ octahedra are linked in a regular cubic array forming the high-symmetry $Pm3m$ prototype in the paraelectric state. In the ferroelectric state below the Curie temperature $T_C = 110$ °C, a spontaneous polarization arises due to the non-centrosymmetric displacement of Ti⁴⁺ and O²⁻ ions relative to Ba²⁺ ions ($P4mm$). The Landau coefficients, elastic, electro-mechanical, and thermal properties of BT are well known (see Table 1) [13,14] that allows us to carry out a numerical quantitative study. We note that in the temperature range from $T_1 = 107$ °C to $T_2 = 109$ °C in which we are running our calculations, the heat capacity and

Table 1
Thermodynamic coefficients, elastic, thermal and chemical constants of BT [13,14]

Coefficient/constant	Unit	Value	Reference
C	°C	1.71×10^5	13
T_C	°C	110	13
a_{11}	m^5/C^2F	$3.6(T-175) \times 10^6$	13
a_{111}	m^9/C^4F	6.6×10^9	13
C_{11}	N/m^2	1.76×10^{11}	13
C_{12}	N/m^2	8.46×10^{10}	13
Q_{12}	m^4/C^2	-0.043	13
k (at 108 °C)	J/ms K	4.5	14
ρ (at 108 °C)	kg/m ³	6.02×10^3	14
C_p (at 108 °C)	J/mol K	115	14

thermal conductivity change slightly for homogeneous BT and are taken as 115 J/mol K and 4.5 J/ms K, respectively [14].

We first proceed with a calculation of the evolution of the temperature gradient through the material right after the temperature change of the IR-exposed surface from T_1 to T_2 . The temperature profile across the ferroelectric can be obtained via Eq. (3), which can be solved numerically using a finite difference method (FDM) by dividing the sample into N infinitesimally small layers with thickness of $h = L/N$ and the initial and boundary conditions shown in Fig. 1. Subsequently, Eq. (8) can be evaluated via FDM using the temperature profile obtained from the heat transfer analysis. This results in a time-dependent polarization profile within the BT sample. Thus, the charge accumulation on an amplifier sense capacitor required for the evaluation of the dynamic pyroelectric response can be calculated based upon this polarization profile using basic electrostatics for each time step [8]

$$\Delta Q = C_Q V_{int} = \frac{\eta}{L} \int_0^L z \left(\frac{dP(z)}{dz} \right) dz \quad (10)$$

where C_Q is the capacitance of the amplification circuit, V_{int} is the built-in potential due to the bound charge due to the polarization gradient, and η is the ratio of C_Q to the capacitance of the ferroelectric sample, C_F . From Eq. (10), we can also determine V_{int} . For the i th layer, the charge can be expressed as $\Delta Q = [(P_{i+1} - P_i)/h]Ah$, since the layer is infinitesimally small. Here, P_i is the polarization at the i th layer. Substituting this equation into $V = \Delta Qh/\epsilon A$ for the potential between two parallel plates yields the voltage across the i th layer

$$V_i = \frac{\Delta Q_i h}{\epsilon_i A} = \frac{(P_{i+1} - P_i)h}{\epsilon_i}, \quad (11)$$

where ϵ_i is the dielectric permittivity of the i th layer. For the N separate layers, the total potential can be found by summing the potentials of each layer:

$$V_{int} = \sum_1^N \frac{(P_{i+1} - P_i)h}{\epsilon_i}. \quad (12)$$

A ‘dynamic’ enhancement in pyroelectric coefficient can then be defined as the change in charge accumulated on the amplification capacitor as a result of the temperature variation between the initial and final state, $p_D = \partial(\Delta Q)/\partial T$ [15]. The charge difference is an immediate consequence of the polarization gradient across the sample and resultant internal potential defined by Eqs. (10) and (12), respectively. The polarization gradient itself is a function of the time-dependent temperature gradient and it is thus expected that p_D will change in time as thermal equilibrium is approached, where it will vanish as the polarization inhomogeneity vanishes.

Figs. 2(a) and 3(a) show the temperature variation for samples with $L = 1$ and 100 μm , respectively, as a function of time for the aforementioned 2 °C temperature step. This temperature range is close to, but below the Curie temperature (110 °C), where the highest pyroelectric response would be expected. It is clearly seen from Figs. 2(a) and 3(a) that the rate

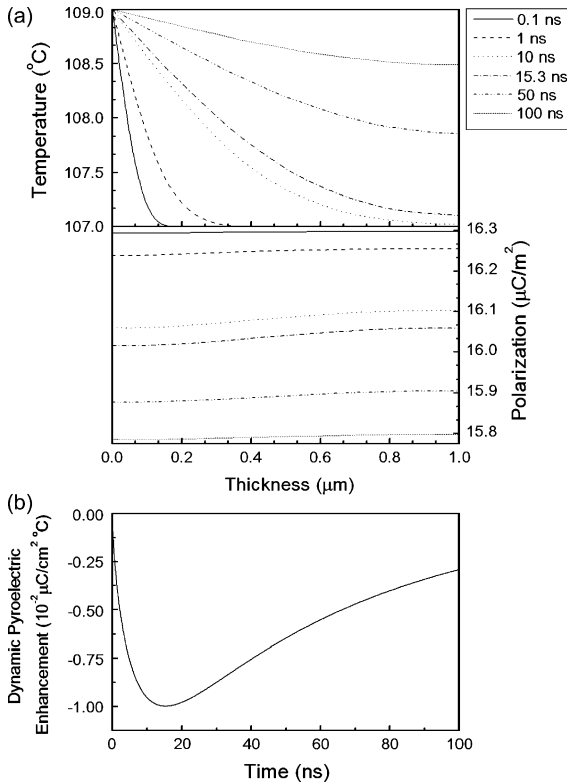


Fig. 2. (a) Temperature gradient across the 1 μm BT sample at different times ($T_1=107^\circ\text{C}$ and $T_2=109^\circ\text{C}$). (b) Polarization gradient across the 1 μm BT sample at different times. (c) Dynamic pyroelectric enhancement as a function of time for a 1 μm BT sample. The pyroelectric peak is $-0.01 \mu\text{C}/\text{cm}^2 \text{ }^\circ\text{C}$ at approximately 15 ns.

of change of temperature gradient is a function of sample thickness. The calculations were carried out until the adiabatic side of the ferroelectric sample reached 108.5°C . While it takes $0.1 \mu\text{s}$ for the surface of a 1 μm sample, which is thermally insulated, to get to 108.5°C , the 100 μm sample reaches this same temperature in 1 ms.

Figs. 2(b) and 3(b) plot the polarization profiles throughout the samples for different times. This polarization gradient is indeed smooth and the change in the polarization from one end to the other is very small, validating our approximation regarding the internal electric field. Even in the case of a large depolarization field, the material would split into electrical domains, which would minimize the depolarization energy. In this case, Eq. (4) would still provide us average properties, but would not be able to explain dynamic behavior such as polarization switching.

The contribution due to the dynamic pyroelectric enhancement is seen in Figs. 2(c) and 3(c) for the 1 and 100 μm samples, respectively. For the 1 μm sample, the dynamic enhancement peaks around 15 ns whereas for the 100 μm sample, the peak is approximately at 140 μs. In both cases the maximum dynamic pyroresponse is approximately $-0.01 \mu\text{C}/\text{cm}^2 \text{ }^\circ\text{C}$.

The similarity in Figs. 2 and 3 can easily be understood if one recalls that the thermal time constant of a thermal system is set by L^2/α , and the length scale set by the thickness of the

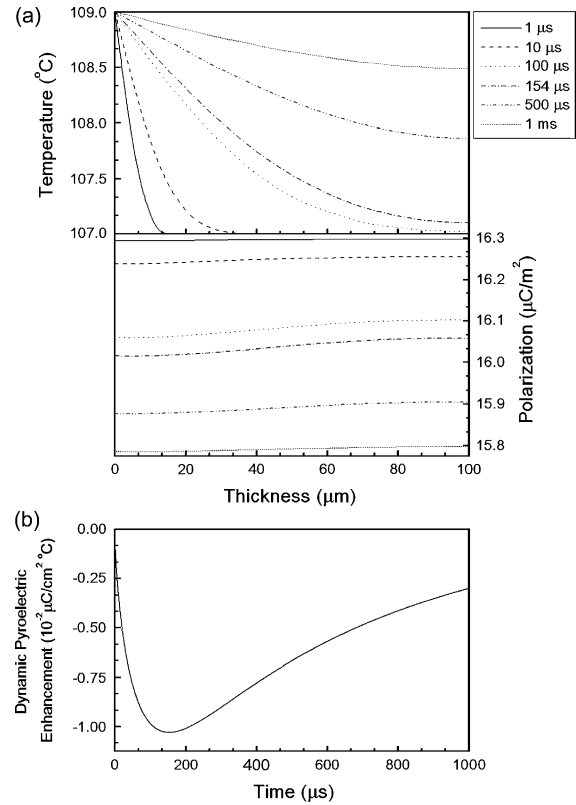


Fig. 3. (a) Temperature gradient across the 100 μm BT sample at different times ($T_1=107^\circ\text{C}$ and $T_2=109^\circ\text{C}$). (b) Polarization gradient across the 100 μm BT sample at different times. (c) Dynamic pyroelectric enhancement as a function of time for a 100 μm BT sample. The pyroelectric peak is $-0.01 \mu\text{C}/\text{cm}^2 \text{ }^\circ\text{C}$ at approximately 150 μs.

sample [16]. In our plots, we have therefore expanded the time scale by a factor of 10^4 , and the length scale by 100 to account for the difference in thicknesses of the two samples, thus yielding virtually identical figures.

The presence of a maximum in p_D can be explained via the evolution of the temperature profile with time. Because the temperature gradient in the ferroelectric is a transient phenomenon, the homogeneous ferroelectric becomes a well-understood temperature-graded ferroelectric possessing a polarization gradient [6]. The dynamic pyroelectric response p_D (or enhancement over and above the conventional response) is a function of the ‘built-in’ potential associated with a graded ferroelectric. Therefore, p_D should display a maximum at the time when the temperature gradient (hence the polarization gradient) across the sample is the largest. It is obvious that the thickness of the sample should affect both the temperature and polarization profiles and their time dependence. In relatively thinner samples, such as the one of 1 μm thickness, the maximum temperature gradient is reached more quickly [Fig. 2(c)] compared to the 100 μm sample [Fig. 3(c)]. These results are in qualitative agreement with experimental observations where the maximum in pseudo-pyroelectric coefficient for compositionally-graded $\text{KTa}_x\text{Nb}_{(1-x)}\text{O}_3$ [15] and $\text{Ba}_x\text{Sr}_{(1-x)}\text{TiO}_3$ [17,18] was found to occur for maximum polarization variation across the sample. This

Table 2
Comparison of our findings in this study with the experimental data in the literature [15,17,18,20–22]

Material	Substrate	Temperature (°C)	Pyroelectric Coefficient ($\times 10^{-2} \mu\text{C}/\text{cm}^2 \text{ } ^\circ\text{C}$)	Reference
$\text{KTa}_x\text{Nb}_{(1-x)}\text{O}_3$	Y_2O_3	40	–1200.0	[15]
$\text{Ba}_{0.64}\text{Sr}_{0.36}\text{TiO}_3$	Pt/Si	25	–18.6	[17]
Compositionally graded $\text{Ba}_x\text{Sr}_{(1-x)}\text{TiO}_3$ ($x=1 \rightarrow 0.7$)	Pt	–10	–6.0	[18], Effective
Compositionally graded $\text{Ba}_x\text{Sr}_{(1-x)}\text{TiO}_3$ ($x=1 \rightarrow 0.7$)	Pt	25	–0.3	[18], Conventional
$\text{Ba}_{0.8}\text{Sr}_{0.2}\text{TiO}_3$	Pt/Ti/SiO ₂ /Si	16	–4.1	[20]
PbTiO_3	Pt/Ti/SiO ₂ /Si	25	–3.5	[21]
PbTiO_3	Pt/Ti/SiO ₂ /Si	492	–175.0	[21]
Compositionally graded $\text{Ba}_x\text{Sr}_{(1-x)}\text{TiO}_3$ ($x=1 \rightarrow 0.7$)	Si	50	–500.0	[22], Effective
BaTiO_3		~25	–8.0	Theoretical, this study, conventional
BaTiO_3		107–109	–30.0	Theoretical, this study, conventional
BaTiO_3		107–109	–1.0	Theoretical, this study, maximum dynamic

latter behavior was quantitatively explained [19] using a similar theoretical thermodynamic analysis as was presented in this study.

The conventional pyroelectric response of homogeneous ferroelectric bulk BT in the same temperature range (107–109 °C) can also be found using standard Landau formalism, yielding a value of $-0.3 \mu\text{C}/\text{cm}^2 \text{ } ^\circ\text{C}$ (see Table 2). This implies that in this small temperature window, one might expect a maximum enhancement in the dynamic response over the static response of only about 3.3%. While this enhancement seems small as compared to the conventional response of BT, it needs to be remembered that these calculations were done relatively far from the Curie temperature, where the effects of the temperature (and polarization) gradients are substantially diminished. The practical operation temperature range of a pyrosensor is usually within $\pm 0.05 \text{ } ^\circ\text{C}$ of the Curie temperature. Unfortunately, theoretical analysis at a ferroelectric Curie temperature (where most pyroelectric sensors traditionally operate) is problematic due to the singularity in the permittivity. For other ferroelectric material systems, a more substantial enhancement of the total response may be observed (see Table 2) [15,17,18,20–22]. This is particularly true for ferroelectric films where the conventional pyroelectric response is greatly diminished due to internal stresses [23]. In addition, the effects of substrate stress and its alleviation or augmentation, at the Curie temperature can profoundly alter the relative magnitudes of both the conventional pyroelectric coefficient and its dynamic enhancement.

It must also be pointed out, that the enhancement factors will only be observable from dynamic pyroelectric measurements. As indicated in Figs. 2(c) and 3(c), this contribution vanishes when thermal equilibrium is reached; hence, a possible reason why the discrepancies between the dynamic and quasi-static pyroelectric coefficient are most observable in bulk ferroelectric materials, where the thermal time constants are relatively long. For thin film ($< 1 \mu\text{m}$) pyroelectric detectors, these enhancements would be totally missed as the

maximum augmentation occurs on the time scale of nanoseconds, well short of typical integration and chopper times.

Finally, Eq. (10) clearly indicates that the contribution from the dynamic enhancement can be greatly augmented through change in amplification capacitance, i.e. by changing the capacitance ratio, η , which was taken as 1 in this study. Increasing the value of this ratio would further improve the dynamic contribution and the overall pyroelectric response as was done to good effect for compositionally graded $\text{KTa}_x\text{Nb}_{(1-x)}\text{O}_3$ and $\text{Ba}_x\text{Sr}_{(1-x)}\text{TiO}_3$, see Table 2.

Acknowledgements

The work at the University of Connecticut was supported by the National Science Foundation (NSF) under Grant No: DMR-0132918.

References

- [1] J. Cooper, Rev. Sci. Instrum. 33 (1962) 92.
- [2] R.W. Whatmore, P.C. Osbond, N.M. Shorrocks, Ferroelectrics 76 (1987) 351.
- [3] S.B. Lang, Phys. Today (2005) 31.
- [4] B.M. Kulwicki, A. Amin, H.R. Beratan, C.M. Hanson, Ferroelectric Imaging, New York 1992 (IEEE), p. 1.
- [5] R. Watton, Ferroelectrics 91 (1989) 87.
- [6] W. Fellberg, J. Mantese, N. Schubring, A. Micheli, Appl. Phys. Lett. 78 (2001) 524.
- [7] S.P. Alpay, Z.G. Ban, J.V. Mantese, Appl. Phys. Lett. 82 (2003) 1269.
- [8] Z.-G. Ban, S.P. Alpay, J.V. Mantese, Phys. Rev. B 67 (2003) 184104.
- [9] S. Zhong, S.P. Alpay, J.V. Mantese, Appl. Phys. Lett. 87 (2005) 102902.
- [10] A.L. Roytburd, S. Zhong, S.P. Alpay, Appl. Phys. Lett. 87 (2005) 092902.
- [11] L.B. Freund, J. Mech. Phys. Solids 44 (1996) 723.
- [12] A.L. Roytburd, J. Slutsker, Acta Materialia 50 (2002) 1809.
- [13] N.A. Pertsev, A.G. Zembilgotov, A.K. Tagantsev, Phys. Rev. Lett. 80 (1998) 1988.
- [14] K.-H. Hellwege, A.M. Hellwege, Landolt-Bornstein, Numerical Data and Functional Relationships in Science and Technology, vol. 16, Springer, Berlin, 1981.
- [15] N.W. Schubring, J.V. Mantese, A.L. Micheli, A.B. Catalan, R.J. Lopez, Phys. Rev. Lett. 68 (1992) 1778.

- [16] H.S. Carslaw, J.C. Jaeger, *Conduction of Heat in Solids*, Oxford University Press Inc., New York, 1986. pp. 99–104.
- [17] T. Zhang, H. Ni, *Sens. Actuators A* 100 (2002) 252.
- [18] M.S. Mohammed, G.W. Auner, R. Naik, J.V. Mantese, N.W. Schubring, A.L. Micheli, A.B. Catalan, *J. Appl. Phys.* 84 (1998) 3322.
- [19] S. Zhong, S.P. Alpay, Z.-G. Ban, J.V. Mantese, *Appl. Phys. Lett.* 86 (2005) 092903.
- [20] J.-C. Cheng, J. Tang, J.-H. Chu, A.-J. Zhang, *Appl. Phys. Lett.* 77 (2000) 1035.
- [21] C. Shi, L. Meidong, L. Churong, Z. Yike, J.D. Costa, *Thin Solid Films* 375 (2000) 288.
- [22] F. Jin, G.W. Auner, R. Naik, D.W. Schubring, J.V. Mantese, A.B. Catalan, A.L. Micheli, *Appl. Phys. Lett.* 73 (1998) 2838.
- [23] Z.-G. Ban, S.P. Alpay, *Appl. Phys. Lett.* 82 (2003) 3499.